Circulation within the Ocean Storms Area Located in the Northeast Pacific Ocean Determined by Inverse Methods

R. J. MATEAR

Department of Oceanography, University of British Columbia, Vancouver, British Columbia, Canada

(Manuscript received 30 September 1991, in final form 1 June 1992)

ABSTRACT

An inverse model was applied to hydrographic data obtained from a cruise in the autumn of 1987 in a small area (300 × 250 km) in the northeast Pacific Ocean. The inverse model used geostrophy and a linear β-plane vorticity equation as dynamical constraints. The conservation of mass and the steady-state advection–diffusion equations for temperature and salinity were used to form a set of equations from which the reference level velocities and mixing terms were determined. Additional constraints were included in the model by forcing the horizontal velocity from the model to be consistent with bouy data from the near surface.

The vertical mixing coefficients determined by the model increased from zero at 150 m to 14 $cm^2 s^{-1}$ at 1500 m. The horizontal diffusivity displayed a minimum at 500 m of 1000 $m^2 s^{-1}$ and increased to 5300 $m^2 s^{-1}$ at 150 m. A middepth maximum of 6000 $m^2 s^{-1}$ was observed at 900 m before decreasing to zero at 1500 m. The calculated vertical velocities were weak functions of depth changing by less than 3.0×10^{-6} m s^{-1} between 150 m and 1500 m, showing the horizontal velocities to be nearly nondivergent.

The geostrophic flow field determined from the inverse model was generally smooth, exhibiting well-defined flow features. The horizontal flow did not indicate a depth of no motion in the study area. The comparison of a 7-day average of current meter observations with inverse velocities showed that the two velocity measurements were consistent at 500 m. The difference between the two velocities increased as one moved upward from 500 m and downward to 1000 m. The increases in the velocity differences agreed with the calculated horizontal diffusivities, which implied enhanced eddy activity in the upper ocean and at middepths.

1. Introduction

In the fall of 1987, the Ocean Storms Experiment (OSE) was carried out in the northeast Pacific Ocean to study the interaction of the atmosphere with the ocean during severe storms. One component of this experiment was to obtain hydrographic data on a grid of stations in the OSE area. The study area was the open ocean, 1000 km west of Vancouver Island, centered at 47.5°N, 139.0°W (Fig. 1). This area of the ocean has been the focus of previous studies, some of which sought to better understand the exchanges of momentum, heat, and mass between the atmosphere and the ocean [e.g., Storm Transfer and Response Experiment, Fleagle et al. (1982)], while others aimed at understanding the hydrographic structure of the ocean in this area (e.g., Tabata 1965, 1976). The unique feature of the conductivity–temperature–depth (CTD) data presented in this paper is that the data were collected on a relatively fine grid providing good spatial resolution. Data from one oceanographic cruise in October 1987 completed a grid of 30 stations to a depth of 1500 dbar in the OSE area.

This paper describes the use of an inverse model to determine the general circulation in the OSE area from the hydrographic and drifter data. A companion paper (Matear et al. 1992) provides a description of the oceanographic conditions based on this hydrographic data and closes the heat and salt budgets of the upper ocean. The organization of this paper is as follows. After a brief description of the datasets in section 2, the inverse model is developed in section 3. In section 4, the model is evaluated to determine the uncertainty of the calculated unknowns. Section 5 presents the circulation parameters calculated from the model. The model results are compared to current meter observations and Lagrangian drifters. Section 6 presents a summary.

2. Oceanographic datasets

a. CTD profiles

In the Ocean Storms area, CTD data were collected on a six station by five station array with grid spacings of 60 km (Fig. 1). The array was designed to resolve mesoscale features expected in this area (Fofonoff and Tabata 1966). The data was acquired from 30 September to 7 October 1987 using the CRV *Parizeau* (Tabata et al. 1988), and the temperature and salinity values were interpolated to a constant pressure interval of 1 dbar. To smooth any random errors present in the

Corresponding author address: Richard J. Matear, Centre for Climate Chemistry, Institute of Ocean Sciences, Sidney, British Columbia, Canada V8L 4BZ.

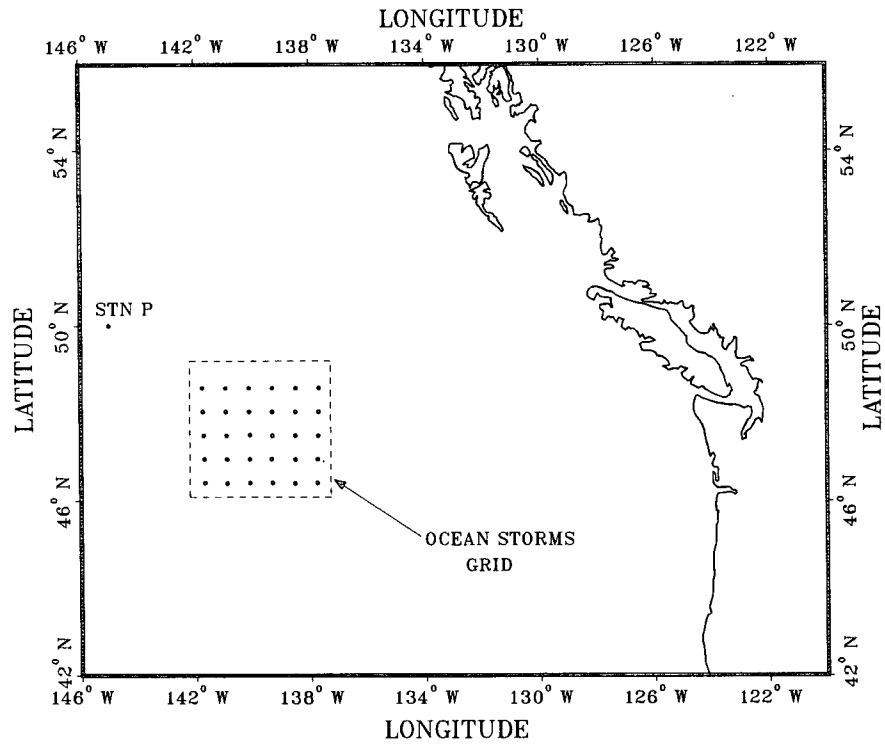

FIG. 1. Location of the Ocean Storms Experiment grid.

temperature and salinity values, a 10-m running average filter was applied to the upper 500 m, and a 20-m running average filter was applied to the remaining depths. Dynamic height was determined from the filtered values of temperature and salinity (Fofonoff and Millard 1983).

b. *TriStar drifters*

The trajectories of 37 TriStar bouys deployed at the Ocean Storms site in early October 1987 were used to constrain the near-surface low-frequency flow (D'Asaro et al. 1993). The buoys were drogued at 15 m. The bouy trajectories were demodulated into subinertial and inertial currents by D'Asaro et al. (1993) using a filtering parameter $8/f$ seconds, which suppresses frequencies above about 0.2 cycles per day. Combining the wind-forced and demodulation errors, D'Asaro et al. (1993) estimate the 15-m subinertial, non-wind-forced velocities to about 0.15 m s^{-1}. Figure 2 shows the low-frequency velocities sampled every 4 days for all TriStar drifters in the OSE array for 30 September to 20 October (days 280–300). A pattern of northward and eastward flow with embedded eddies is apparent. With minor exceptions, nearby velocity vectors point in nearly the same direction, which suggests that the bouy motions mostly reflect a steady velocity pattern and that neither wind effects nor evolution of the low-frequency velocity field is important (D'Asaro et al. 1993). From the velocity field, D'Asaro et al. (1993) calculated the dominant scale L to be 50–100 km, close to the expected mesoscale eddies, with an associated

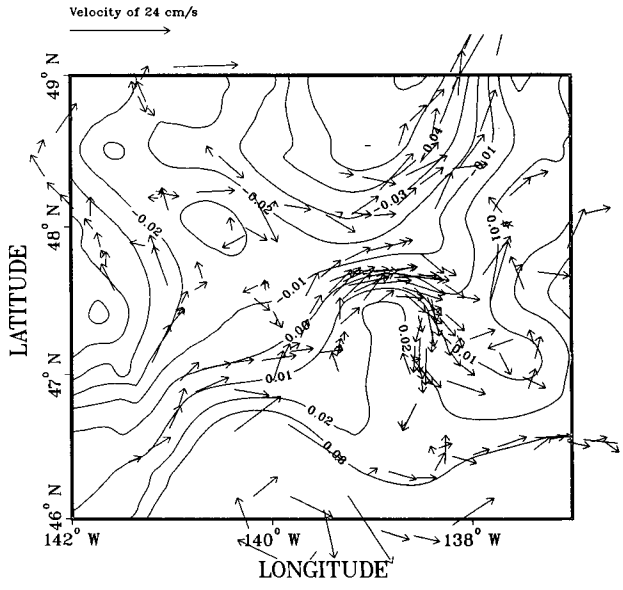

FIG. 2. The subinertial velocities from all TriStar drifter sampled every 4 days for days 280–300 of 1987. Superimposed on these velocities are the dynamic height contours in dynamic centimeters computed from objective analysis of the drifter data (D'Asaro et al. 1993).

Rossby number, U/fL, of less than 0.02. The flow should therefore be geostrophic and thus nearly nondivergent. For use in the inverse model the low-frequency drifter velocities in Fig. 2 were objectively mapped to obtain dynamic height. The calculation of dynamic height was performed by D'Asaro et al. (1993) and is included in Fig. 2.

c. *Current mooring*

A current meter moored in the center of the OSE area at 47.5°N, 139.3°W provided current meter observations and high-frequency temperature fluctuations during the collection of the CTD data. The current meter observations from this mooring were provided by M. Levine and C. Paulson of Oregon State University. In the upper part of the mooring, seven Vector Measuring Current Meters (VMCM) were distributed from 60 m to 195 m. The lower part of the mooring included five Aanderaa meters distributed from 500 m to 4000 m. High-frequency temperature measurements were made at 175 m, 224 m, 300 m, 375 m, 500 m, 1000 m, and 2000 m. The dominant signal in this data is the semidiurnal internal tide that appears at all depths. The phase of the internal tide is not constant, and the amplitude of the oscillation is highly variable in time (M. Levine, personal correspondence). The fluctuation of the temperature data was used to estimate the non-steady-state errors in the CTD data and to assess the effect of these errors on the inverse solution.

3. Developing and solving the inverse problem

a. *Model equations*

Assuming hydrostatic balance and geostrophy, one obtains the horizontal geostrophic velocities (u, v) by integrating the thermal wind equations vertically from a reference depth, z_r, to obtain

$$v = -\frac{g}{\rho_0 f}\int_{z_r}^{z} \rho_x dz + v_0 = v_r + v_0 \qquad (1)$$

$$u = \frac{g}{\rho_0 f}\int_{z_z}^{z} \rho_y dz + u_0 = u_r + u_0. \qquad (2)$$

The horizontal velocities are made up of two terms, the velocities at the reference level (u_0, v_0) and the relative velocities (u_r, v_r). The reference level velocities are unknown, while the relative velocities were calculated from the horizontal gradients of the density field (ρ_x, ρ_y) derived from the hydrographic data. In accordance with the relatively small scale of circulation in the region, the Coriolis parameter was defined by the β-plane approximation $(f = f_0 + \beta y)$, where f_0 is constant and β is the change in f with latitude $(\beta = \partial f/\partial y)$. From the horizontal divergence of the geostrophic velocities, $(u_x + v_y)$, a linear β-plane vorticity equation was obtained:

$$\beta v = f w_z. \qquad (3)$$

By using the vorticity equation in the definition of the vertical velocity, (w), the inverse model tries to conserve potential vorticity. Integrating Eq. (3) from a reference level, z_r, gives

$$w = \frac{\beta}{f}\int_{z_r}^{z} v dz + w_0, \qquad (4)$$

and substituting (1) for v gives

$$w = \frac{\beta}{f}\int_{z_r}^{z} v_r dz + \frac{\beta}{f} v_0(z - z_r) + w_0$$

$$= w_r + \frac{\beta}{f} v_0(z - z_r) + w_0. \qquad (5)$$

To evaluate these unknown reference velocities, u_0, v_0, and w_0, the equations for conservation of mass and conservation of salt and heat were used. The equations for conserving salt and heat are defined by the following advection–diffusion equations for salinity (S) and temperature (T):

$$\nabla\cdot(\mathbf{u}S) - \nabla\cdot(k\nabla S) = 0, \qquad (6)$$

$$\nabla\cdot(\mathbf{u}T) - \nabla\cdot(k\nabla T) = 0. \qquad (7)$$

The vector $\mathbf{u}$ represents the three velocity components, and k is the mixing coefficient. In a stratified ocean, isopycnal mixing is much stronger than diapycnal mixing (Olbers et al. 1985). In the OSE array, the slopes of the isopycnal surfaces were almost horizontal and varied by less than 100 m over 300 km. This enabled one to replace the isopycnal and diapycnal mixing coefficients by vertical and horizontal mixing coefficients, k_z and k_h, respectively. Because of the small area covered by the data (250 km by 200 km), the mixing coefficients were only considered to be functions of depth.

Equations (6) and (7) assume the ocean to be steady state with no sources or sinks. This assumption is clearly violated in the upper ocean. From temperature and salinity profiles taken two months apart in the OSE area (Matear 1989), the valid upper limit chosen for the approximation was 150 m. A profiling current meter moored in the area from August to January showed that the effects of the storms were confined to the upper 150 m of the ocean (Erickson, personal correspondence). The 4 October storm that passed through the area midway through the collection of the CTD profiles altered the conditions in the upper 100 m while imposing little effect on the conditions below 100 m. The steady-state assumption below 150 m can be violated by non-steady-state processes, such as baroclinic eddies and internal gravity waves. These processes can be thought of as features not resolved by the model. The effect that non-steady-state processes have on the solution will be investigated in the section on evaluating the model and solution.

TABLE 1. The levels used to vertically define the boxes used in the model.

Level	Depth (dbar)	Depth (m)
1	150	149.1
2	200	198.8
3	250	248
4	300	298
5	400	397.1
6	500	496.2
7	600	695.2
8	700	694.2
9	800	793.1
10	900	892.0
11	1000	990.8
12	1200	1188.3
13	1500	1484.2

The surface geostrophic velocity was further constrained in the model by using the dynamic height calculated from objectively mapping the drifter velocities. The surface constraint on the geostrophic flow forced the inverse solution to agree with the buoy data while trying to conserve mass, heat, and salt. The additional constraints on the horizontal reference velocities allowed one to better estimate the mixing coefficients and to better assess the effect of non-steady-state processes on the solution.

b. System of equations

To develop a set of equations from the continuity equations, the ocean was divided into boxes bounded horizontally by four hydrographic stations and vertically by two depth surfaces. Traditionally, in the large regional studies (Wunsch 1978; Wunsch and Minister 1982), the vertical layering was based on isopycnal surfaces. The use of this layering stems from the idea that flow preferentially moves along isopycnal surfaces (Montgomery 1938). In a small regional study such as the Ocean Storms Experiment, the slopes of the isopycnal surfaces were nearly horizontal, with a change of isopycnal depth of less than 100 m over 300 km. It was, therefore, considered appropriate and convenient to divide the ocean vertically according to pressure surfaces (Table 1), instead of isopycnal surfaces. These surfaces of constant pressure were almost identical to surfaces of constant depth (±0.1 m). The ocean was divided vertically into 12 layers between 150 m and 1500 m. The hydrographic stations divided the OSE array horizontally into 20 regions. The division of the ocean into boxes produced 240 boxes for the OSE area.

The velocity and the mixing coefficients on each face of the box were resolved by the inverse model. The model determined 24 u_0, 25 v_0, 20 w_0, 12 k_h, and 13 k_z. The total number of unknowns to the problem was 94. These unknowns were determined from a set of equations generated from the three continuity constraints and the velocity constraints. One equation was obtained from the conservation of mass by integrating the mass equation around the volume enclosed by one of the boxes:

$$\iiint (\nabla \cdot \mathbf{u})dV = \iint \mathbf{u} \cdot \mathbf{n}dA = \Delta y \Delta z (u_0|_E^W) + \Delta x \Delta z (v_0|_S^N) + \Delta x \Delta y (w_0|_B^T) + \Delta y \Delta z (\bar{u}_r|_E^W) + \Delta x \Delta z (\bar{v}_r|_S^N) + \Delta x \Delta y (\bar{w}_r|_B^T) = 0. \quad (8)$$

The vector $\mathbf{n}$ is the unit vector normal to each box face. The values Δx, Δy, and Δz correspond to the x, y, and z dimensions of the box. The overbar denotes the averaging of relative velocities (u_r, v_r, and w_r) through the corresponding box face, with the subscripts E, W, N, S, T, and B referring to the east, west, north, south, top, and bottom faces of the box.

An equation for the conservation of salt, S, was similarly obtained by integrating Eq. (6) around the volume enclosed by a box:

$$\iiint \nabla \cdot (\mathbf{u}S)dV - \iiint \nabla \cdot (k \nabla S)dV = \iint (\mathbf{u}S \cdot \mathbf{n})dA - \iint (k \nabla S \cdot \mathbf{n})dA$$
$$= \Delta y \Delta z (u_0 \bar{S}|_E^W) + \Delta x \Delta z (v_0 \bar{S}|_S^N) + \Delta x \Delta y (w_0 \bar{S}|_B^T) + \Delta y \Delta z (\bar{u}_r \bar{S}|_E^W) + \Delta x \Delta z (\bar{v}_r \bar{S}|_S^N) + \Delta x \Delta y (\bar{w}_r \bar{S}|_B^T) - \Delta x \Delta y \left(k_z \frac{\overline{\partial S}}{\partial z}\Big|_B^T \right) - \Delta y \Delta z \left(k_h \frac{\overline{\partial S}}{\partial x}\Big|_E^W \right) - \Delta x \Delta z \left(k_h \frac{\overline{\partial S}}{\partial y}\Big|_S^N \right)$$
$$= 0. \quad (9)$$

This equation relates the unknown transport of salinity (S) due to the reference velocities and mixing terms to the known transport of S due to the relative velocities. The advective transports were calculated by multiplying the average salinity value on the box face by the average velocity through the box face. The mixing transports were calculated by multiplying the average gradient of salinity normal to the box face by the corresponding mixing coefficient on the box face. An identical equation for the conservation of heat was obtained by replacing S in (6) with T.

By applying these equations to all of the defined boxes, a set of equations, $\mathbf{Ax} = \mathbf{b}$, was generated. The vector **x** represents the unknown variables u_0, v_0, w_0, k_z, and k_h; the matrix **A** represents the average properties on the faces of the boxes; and the vector **b** represents the mass, salt, and temperature transport due to the relative velocities. For the box configuration described above, there were 720 equations to constrain the 94 unknowns. Averaging the variables on each face of the box resulted in a reduction in the resolution of the model and the susceptibility of the inversion to errors in the data caused by differentiating the continuity equations (Wunsch 1985).

The velocity constraints required that the absolute geostrophic velocities at 15 m, calculated from the drifters' dynamic height map (u_{drifter}, v_{drifter}), must equal the geostrophic velocities calculated from the inverse model at 15 m. The equations used were

$$u_0 + u_r = u_{\text{drifter}} \tag{10}$$

$$v_0 + v_r = v_{\text{drifter}}. \tag{11}$$

The velocity constraints provided 49 additional equations to the inverse model.

c. *Including a priori information*

Additional information was included in the inverse problem through the use of weighting matrices and inequality constraints to obtain a more realistic solution. To remove any biases in the solution, the inverse problem was weighted so as to treat all equations and unknowns equally (Wunsch 1978; Tziperman and Hecht 1988). The weighted problem can be written as

$$\mathbf{QAW}\,\mathbf{W}^{-1}\mathbf{x} = \mathbf{Ob}$$

$$\mathbf{B}\qquad\mathbf{m}\quad = \mathbf{e}. \tag{12}$$

The matrices **Q** and **W** are the data-weighting matrix and the parameter-weighting matrix, respectively.

The data-weighting matrix was defined to be a diagonal matrix equal to the row norm of **A**. Such a weighting forced all equations to be treated equally (Wiggins 1972). The data-weighting matrix, **Q**, was defined as follows:

$$Q_{ii} = \Big[\sum_{j=1}^{M} a_{ij}^2\Big]^{-1/2}, \tag{13}$$

with a_{ij} being the elements of **A**, and M the number of unknowns.

The parameter-weighting matrix **W**, used to include information on the expected magnitude of the different model parameters (Wiggins 1972), was defined as a diagonal matrix

$$W_{jj} = |x_j|^{1/2}\Big[\sum_{i=1}^{N} a_{ij}^2\Big]^{-1/4}, \tag{14}$$

with x_j being the expected magnitude of the jth unknown and N the number of equations. The expected magnitudes of the unknowns were set to $|u_0|$ and $|v_0| = 10^{-2}\ \text{m s}^{-1}$, $|w_0| = 10^{-6}\ \text{m s}^{-1}$, $|k_z| = 10^{-4}\ \text{m}^2\ \text{s}^{-1}$, and $|k_h| = 10^4\ \text{m}^2\ \text{s}^{-1}$. The use of the parameter-weighting matrix forced all the model parameters to be of the same order of magnitude and, thus, not bias the unknowns of large magnitudes (Wiggins 1972).

Inequality constraints were included in the model to force the mixing coefficients to be positive (Olbers et al. 1985). This extension is called the least-squares inversion with inequality constraints (LSI) (Lawson and Hanson 1974) and was obtained by minimizing

$$\mathbf{\Phi} = \|B\mathbf{m} - \mathbf{e}\| \tag{15}$$

subject to the inequality constraints

$$\mathbf{Hm} \geqslant 0, \tag{16}$$

with the matrix **H** being defined to allow only positive mixing coefficients.

d. *Solving the inverse problem*

The inverse problem was solved using the LSI algorithm developed by Lawson and Hanson (1974), which involves the singular-value decomposition (SVD) of the matrix **B**. To gain additional insight into the ability of the model to predict a solution, the problem was analyzed using SVD without the inequality constraints. The SVD provided an excellent way to represent and rank the information contained in the matrix B (Wiggins 1972).

The SVD solution to the problem, $\mathbf{Bm} = \mathbf{e}$, was

$$\mathbf{m} = \mathbf{B}^{-1}\mathbf{e} = \mathbf{V\Lambda}^{-1}\mathbf{U}^{\mathrm{T}}\mathbf{e}. \tag{17}$$

The matrix **U** contained k eigenvectors associated with the span of the column vectors of matrix **B**; **V** contained k eigenvectors associated with the span of the row of matrix **B** (Menke 1984); **Λ** was a diagonal matrix of k singular values, arranged in descending order.

To use the generalized inverse equation (17), one must determine the rank of matrix **B** (Menke 1984). To determine the rank of matrix **B** the following were used: 1) a plot of the magnitude of the singular value versus the index number, 2) a plot of the error reduction versus the number of singular values used, and 3) a trade-off curve relating the size of the model variance to the resolution of the model. The rank of **B** was chosen so that singular values smaller than $10^{-5}\ \lambda_{\max}$ were set to zero. The use of the $10^{-5}\ \lambda_{\max}$ cutoff made the matrix **B** full rank and allowed the LSI routine to be used to solve the problem.

4. Evaluating the model and solution

To assess how well the inverse model performed, the sensitivity of the solution was evaluated to the following conditions: 1) the choice of the reference level, 2) the

selected unknown parameters, and 3) the unresolved features in the model. To compare the solutions, a reference solution was determined based on the 12-layer model with the reference level at 1000 dbar. The choice of the 1000-dbar level was based on previous work done in the area (Tabata 1961).

a. The sensitivity of the solution to the choice of reference level

To assess the sensitivity of the solution to the specified reference level, solutions were obtained with several different reference levels. The results showed that the solution was independent of the chosen depth of the reference level.

b. The importance of the different unknown parameters on the solution

The parameter resolution matrix ($\mathbf{VV}^T$) calculated from the SVD analysis, showed that all unknown parameters were well resolved (the diagonal elements of the parameter-resolution matrix were greater than 0.99). The horizontal advection transported most of the salt and heat (75%), while the vertical advection and vertical mixing were approximately equally responsible for transporting the remaining 25%. The horizontal mixing transport of heat and salt was small but did reduce the rms error of the conservation of salt and heat by 2%.

c. Unresolved features in the model and errors in the data

In formulating the model, the steady-state conservation equations for salt and temperature were used. The model cannot resolve any non-steady-state processes, such as Rossby waves or other eddies and internal gravity waves, that were present in the data. To filter the non-steady-state processes from the data was impossible given the temporal and spatial resolution. However, one can indirectly assess the sensitivity of the solution to these processes by perturbing the original T and S data in a manner that attempts to represent the effect these processes have on the data.

The maximum magnitude to perturb the data was based on the high-frequency temperature signal obtained from the current mooring. From this data the maximum perturbation to T and S was estimated to be 0.05°C and 0.01 psu. The maximum isopycnal perturbations were set to 0.01 g cm^{-3}.

Three different perturbation schemes were used to determine the errors to add to the original T and S data: 1) random perturbations, 2) random isopycnal perturbations, and 3) random isopycnal perturbations calculated from the first five internal normal modes determined from the average bouyancy frequency profile of all the data. The T and S errors were determined from the isopycnal perturbations by determining the T and S errors necessary to produce isopycnal perturbations at the corresponding depths in the water column. The first scheme represents the most general case where no information is included on the vertical structure of the perturbations. The second scheme models isopycnal fluctuations, such as internal gravity waves, with no vertical structure. The third scheme represents the kind of vertical structure that one would associate with Rossby waves and internal gravity waves. In the third scheme, five internal normal modes were chosen because, like the high-frequency temperature fluctuations from the mooring, they did not exhibit a discernable depth structure that is more representative of less modes. To include more modes in the third scheme would produce perturbations comparable to the second scheme. The caveat of the perturbation analysis is that one does not have enough knowledge to define the error associated with non-steady-state processes uniquely. The analysis was an attempt to estimate the effect these processes have on the inverse solution.

With the maximum perturbations set, each perturbation scheme was used to determine 20 solutions from which the rms errors were calculated relative to the solution with no perturbation. The results from the three schemes were similar; the mean rms error in the horizontal reference velocities were 0.6 cm s^{-1}; and the mean rms error in the vertical velocities were 2×10^{-6} m s^{-1}. The rms error in the vertical mixing coefficient varied from 0.1 cm^2 s^{-1} at 200 m to 5.8 cm^2 s^{-1} at 1500 m. The rms error in the horizontal mixing coefficient was approximately 1000 m^2 s^{-1} in the upper 600 m of the ocean and 2500 m^2 s^{-1} below 600 m.

The perturbation analysis showed that the errors, introduced by features not resolved by the data, placed limitations on the application of the inverse model to synoptic data. However, equipped with the knowledge of the magnitude of these errors, one can evaluate the solution and compare it with other velocity information that is available.

5. Results of the inverse model

a. The inverse solution

The inverse solution is determined from a 12-layer model using a reference level of 1000 dbar. Data from a depth shallower than 150 m were not used to formulate conservation constraints because this data did not satisfy the steady-state assumptions. The unknown horizontal and vertical reference velocities and the vertical and horizontal mixing coefficients were determined by the inverse model. The solution calculated from the model reduced the error in the conservation of heat and salt by a factor of 10 from a model that assumed the 1000-dbar level was a level of no motion. The rms errors of the inverse model for heat and salt

were 2.1×10^{11} W and 14×10^{6} kg s^{-1}. The model conserves mass to within computer precision. The inverse solutions clearly did not indicate that a depth of no motion existed in the OSE grid.

With the horizontal reference velocities determined, the horizontal velocities in the remainder of the water column were calculated by using the thermal wind equations. The vertical velocities from 150 m to 1500 m were determined by the velocity at the reference level and by integrating the linear β-plane vorticity equation (5).

b. *Vertical and horizontal mixing coefficients*

The inverse solution for the vertical mixing coefficients along with the associate rms errors are shown in Fig. 3. The plot of the vertical mixing coefficients showed that k_z increases with depth. The rms error in the vertical mixing also increased with depth. The increased rms errors are attributed to the weakening of the vertical gradient of temperature and salinity with depth. The structure of the vertical mixing coefficients are comparable to the Gargett (1984) results, which show the vertical mixing to be inversely proportional to the bouyancy frequency. Contrary to these results, Gregg (1989) suggested that the typical thermocline is weakly diffusive and of uniform intensity with depth.

The horizontal mixing coefficient calculated from the inverse model displayed two distinctive features

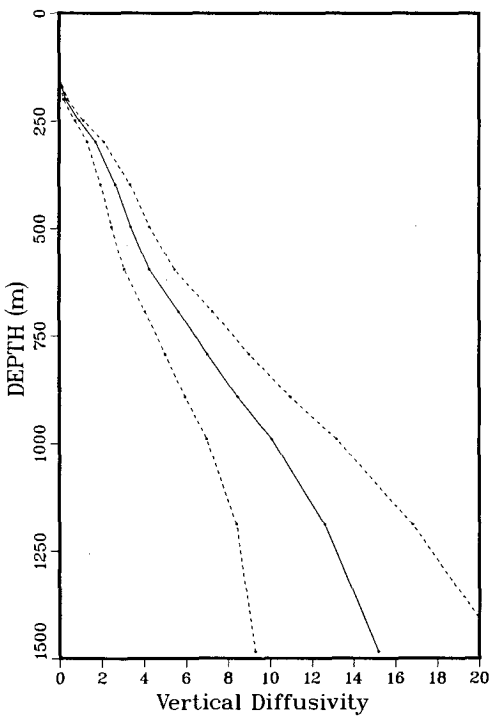

FIG. 3. The vertical mixing coefficients, k_z, determined by the inverse model in units of 10^{-6} m^2 s^{-1}. The solid line shows the inverse solution along with the estimated rms errors (dashed lines).

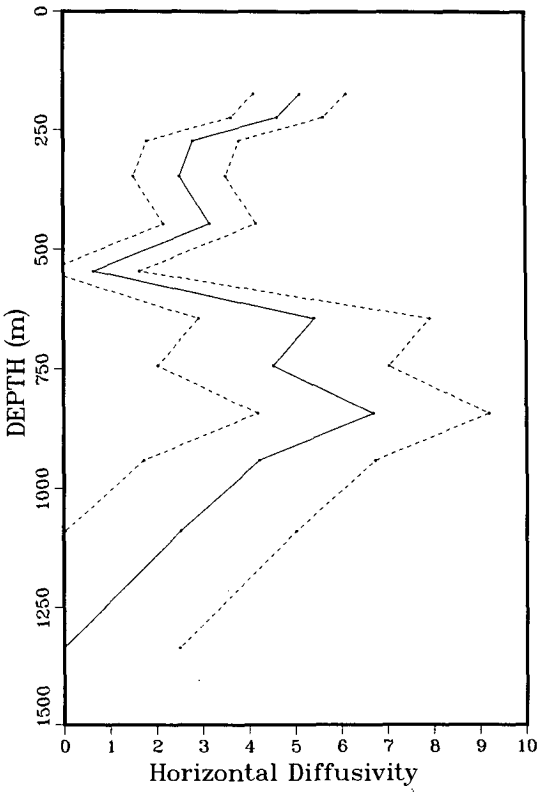

FIG. 4. The horizontal mixing coefficients, k_h, determined by the inverse model in units of 10^3 m^2 s^{-1}. The solid line shows the inverse solution along with the estimated rms errors (dashed lines).

(Fig. 4). In the upper ocean, the horizontal diffusivity decreased from 5200 m^2 s^{-1} at 150 m to 1000 m^2 s^{-1} at 600 m. The decrease in diffusivity with depth suggests a reduction in the eddy energy with depth. The large increase at 650 m to 950 m is difficult to explain but is partially attributed to the limited ability of the model to resolve the horizontal mixing coefficient at these depths. The rms errors below 600 m are 2.5 times greater than errors from the upper 600 m. However, these errors do not completely account for the significant increase in the calculated horizontal diffusivity but suggest an increase in eddy energy at middepths. The effect of the increased mixing terms on the temperature and salinity at middepths is small due to the weak gradients in these tracers at these depths.

c. *Vertical velocity*

The vertical velocity calculated from the model satisfied the β-plane vorticity equation between 150 and 1500 m. The vertical reference velocity ranged from -20×10^{-6} m s^{-1} to 16×10^{-6} m s^{-1}, with and a rms error of 2×10^{-6} m s^{-1}. The vertical-velocity profiles calculated were weak functions of depth, changing by less than 3×10^{-6} m s^{-1} between 150 m and 1500 m. The small change in the vertical velocity with depth

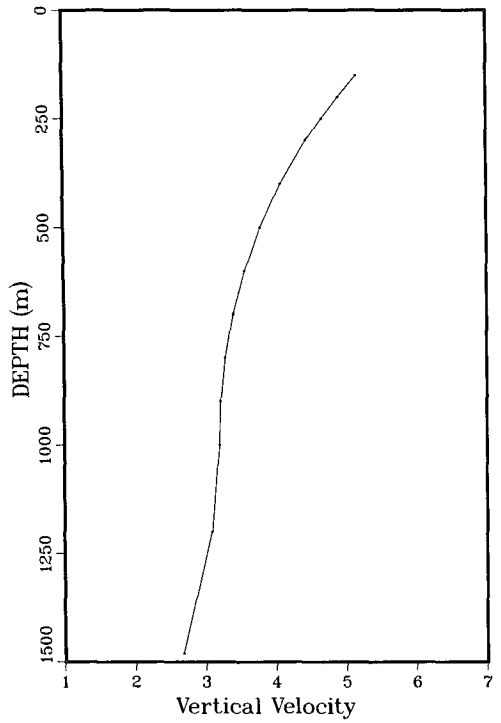

FIG. 5. One profile of the vertical velocity calculated from the inverse model in units of 10^{-6} m s^{-1}; a positive number denotes an upward velocity.

implied that the horizontal flow is nearly nondivergent. An example of a typical profile of the vertical velocity is shown in Fig. 5. The profile shows that most of the change in the vertical velocity is confined to the upper ocean.

The examination of potential vorticity (PV) maps showed that only in the upper 400 m did the PV field possess noticeable structure above the noise level in the data. The horizontal velocities from the inverse model were consistent with the conservation of PV in the upper 400 m of the ocean. Including the conservation of vorticity in the model indirectly through the β-plane vorticity equation adds little useful information to the model from below 400 m. The homogenization of PV in the interior of the ocean suggests that the β effect is not important in the interior of the ocean. The f-plane approximation is valid in the interior of the ocean where the change in vertical velocity is small but fails in the upper ocean.

d. Horizontal velocities

The horizontal velocities determined from the inverse solution represented the "absolute" geostrophic flow field in the Ocean Storms area. The rms error in both components of velocity was approximately ±0.6 cm s^{-1}. This uncertainty in the reference velocities did not greatly alter the flow patterns displayed in the plots. To simplify the discussion of the results, the ocean is divided into three zones, an upper zone (0–200 m), an intermediate zone (200–900 m), and a deep zone (900–1500 m).

The flow in the upper zone of the ocean, Fig. 6, exhibited prominent northeastward flow. Superimposed on this flow were two eddylike features, one in the northwest corner of the grid and the second in the

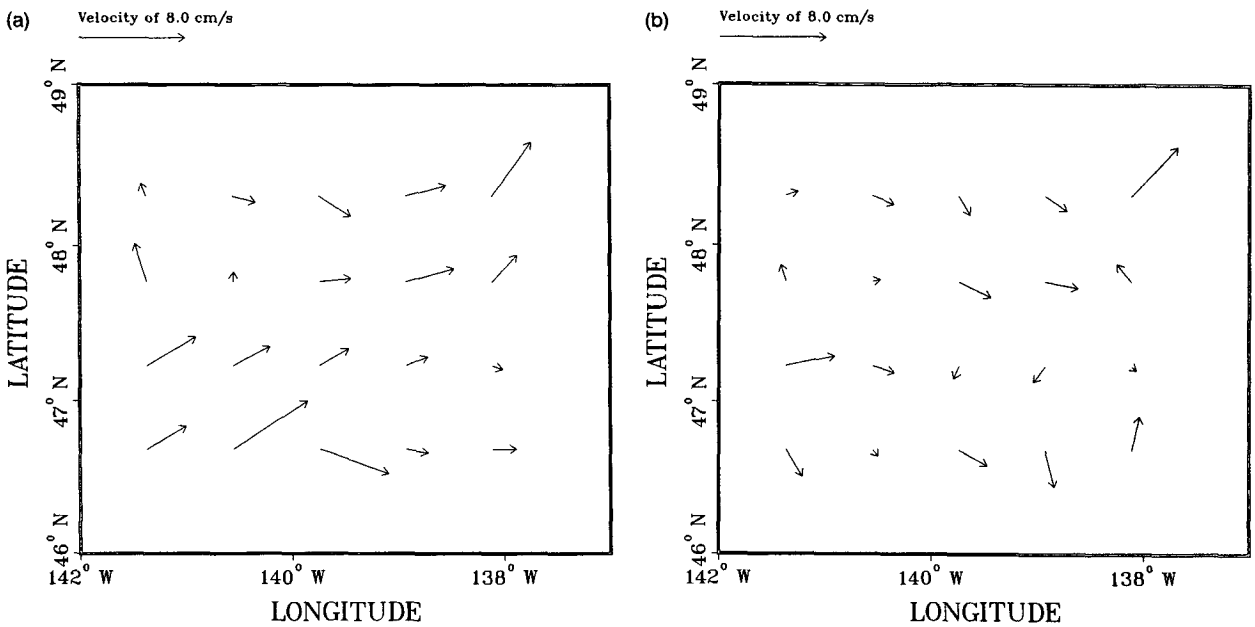

FIG. 6. The geostrophic velocities calculated from the inverse solution at (a) the surface and (b) 200 m.

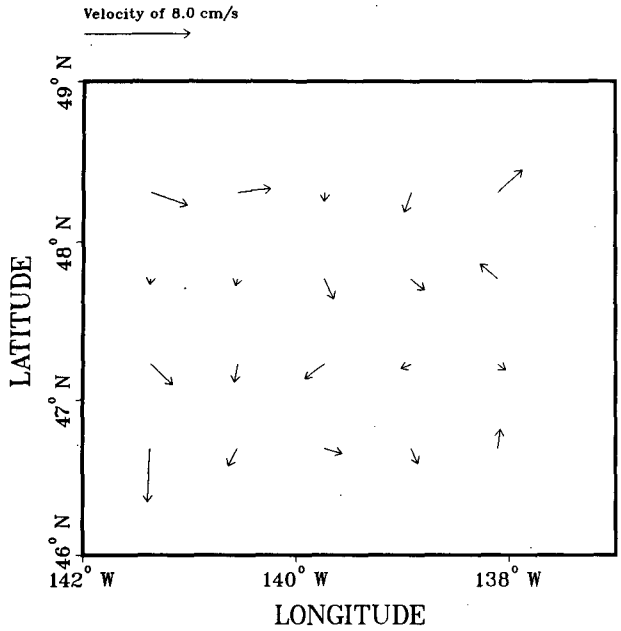

FIG. 7. The geostrophic velocities calculated from the inverse solution at 500 m.

southeast corner of the grid. As one moved down from the surface to deeper levels within this zone the flow rotated southward, and a number of small eddy features developed in the flow. The eddy present in the northwest corner of the grid weakened with depth. The feature in the southeast corner of the grid evolved with depth; what appears as a slight distortion in the flow at the surface developed into a distinct eddy by a depth of 200 m. At this depth, the boundary between the eastward flow in the center of the grid and the southward flow in the southern half of the grid was correlated with an oceanic front observed in the principal halocline in the maps of the temperature and salinity fields (Matear et al. 1992).

In the intermediate zone (Fig. 7), the velocity field had a more coherent and southward flow. A significant northward flow only existed along the eastern edge of the OSE area. In this zone the flow displayed less eddy activity.

In the deep zone (Fig. 8), the southward flow became the dominant feature. At 1000 m, the western half of the grid had a distinct southward flow. Proceeding to 1480 m, a smooth, coherent southward flow pattern began to develop in the entire grid. The flow pattern at 1480 m appeared to be reversed from what was observed at the surface except in the northeast corner of the grid where an eastward flow was still present. The more coherent flow in the deep water further implied a reduction of eddy energy with depth.

e. Drifters and current meter observations

The raw drifter data displayed the three distinct features to the flow (Fig. 2), the two eddies in the northwest and southeast corners of the grid and the generally smooth northeastward flow through the remainder of the grid. The inverse model produced similar features in the calculated flow field but missed much of the eddy activity evident in the bouy data. The bouy data rms velocity for the OSE area was 7 cm s^{-1}, while the inverse solution rms velocity at 15 m gave only 4 cm s^{-1}.

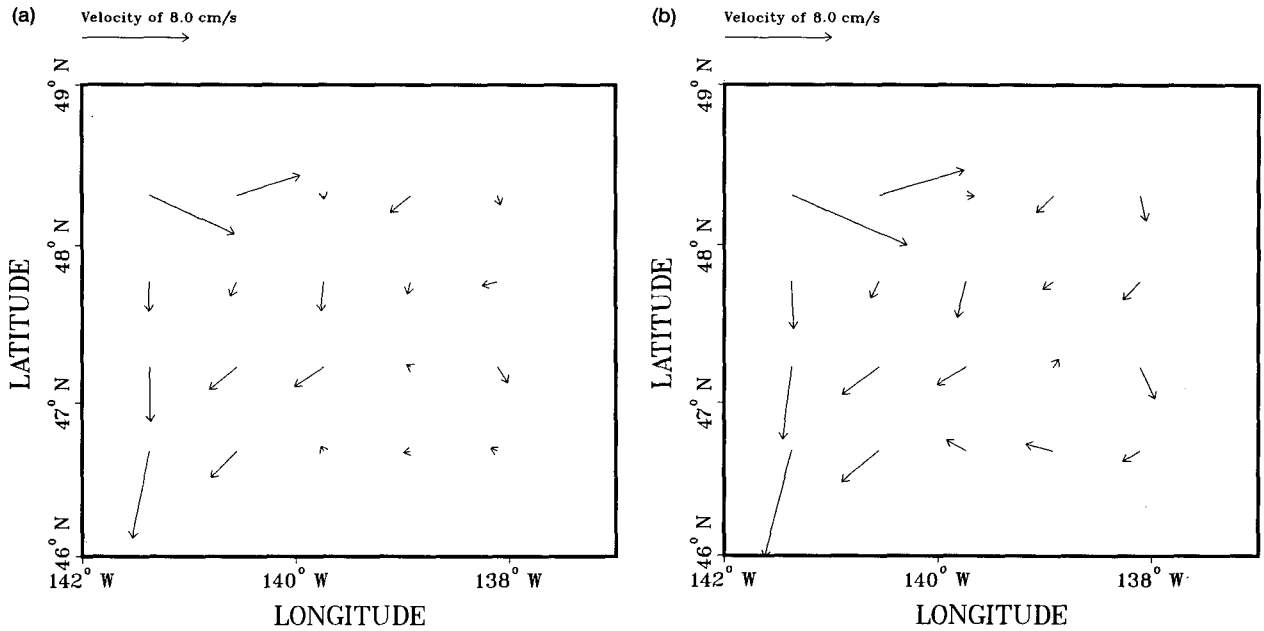

FIG. 8. The geostrophic velocities calculated from the inverse solution at (a) 1000 m and (b) 1480 m.

TABLE 2. A comparison of the 7-day current meter observations from 3 to 9 October 1987 to the geostrophic velocities calculated using the inverse solution. The residual velocities are determined from the difference between the current meter velocities and the geostrophic velocities.

Depth (m)	Current meter velocity (cm s^{-1})		Geostrophic velocity (cm s^{-1})		Residual velocity (cm s^{-1})		
	U	V	U ($\pm$0.6)	V ($\pm$0.6)	U	V	$U^2 + V^2$
1000	−0.24	−0.39	−0.8	−1.6	0.56	1.21	1.78
500	0.34	−0.44	−0.2	−1.0	0.54	0.56	0.61
195	0.14	−0.12	1.2	−0.8	−1.06	0.68	1.59
160	−0.07	−0.56	1.4	−0.7	−1.47	0.14	2.18
140	0.08	0.13	1.7	−0.6	−1.62	0.73	3.16
120	0.67	1.15	2.1	−0.2	−1.43	1.35	3.87
100	2.17	2.39	2.3	0.0	−0.13	2.39	5.73
60	2.36	4.55	2.4	0.5	−0.04	4.05	16.40

To validate the velocities determined from the inverse model and to obtain an estimate of the time scale of geostrophic flow, the model results were compared to the velocity measurements made by current meters moored in the center of the OSE grid, the OSU mooring (at 47.5°N, 139.3°W). To compare with the inverse solution, the current meter observations were averaged for 7 days during the time when the CTD data was collected. The 7-day average of the current meter observations was chosen because it possessed the best agreement with the inverse solution at 500 m and 1000 m. Table 2 summarizes the comparison between the current meter observations and the geostrophic velocities calculated using the inverse model. At a depth of 500 m, the geostrophic velocity was consistent with the average of the current meter observations. A bottom array of pressure gauges deployed in the OSE area was consistent with the 7-day averaging of the current meter observations. The deep geostrophic current measurements inferred from this array were comparable to the current meter observations for periods of a few days to a week (P. Niiler, personal correspondence).

The differences found between the two velocity measurements are mostly attributed to the different spatial sampling of the two velocity measurements. The current meter observations did not provide any information on the spatial structure of the flow; therefore, they capture much more eddy energy than the geostrophic flow determined using the CTD grid. From the raw drifter data, one sees that a strong eddy existed in the vicinity of the current mooring. However, the sampling used in the CTD survey poorly represented this eddy because it was smaller than the grid spacing. The results of the inverse model showed that an eddy feature was present down to 1500 m at the site of the current mooring, making the velocity comparison difficult at all depths.

From the difference between the 7-day averages of the current meter observations and the geostrophic velocities, the residual velocities were calculated (Table 2). The residual velocities were greatest in the upper ocean (60–195 m) and generally decreased with depth. The minimum in the residual velocity occurred at 500 m and the residual velocity increased to the value at 1000 m. The structure of the residual velocity showed similarities with the calculated horizontal diffusivity. The maximum residual velocities showed that the eddy energy in the flow was greatest in the upper 200 m of the ocean and also suggested an increase in eddy energy at 1000 m, consistent with horizontal diffusivity.

6. Conclusions

An inverse box model was applied to the CTD data collected in the northeast Pacific Ocean as part of the Ocean Storms Experiment during fall 1987. The model used geostrophy, the β-plane vorticity equation, conservation of mass equations, steady-state advection–diffusion equations for temperature and salinity, and velocity constraints from bouy data. Mixing in the model was parameterized by depth-dependent vertical and horizontal diffusivities. The inverse solution was consistent with the drifter data and reduced the errors in the conservation of temperature and salinity.

Sensitivity studies of the inverse model showed that the inverse solution was independent of the choice of reference level, but errors arising from unresolved features in the model, such as Rossby and internal gravity waves, were important. The estimated errors in the solution were obtained from perturbation schemes that added errors to the T and S to assess the effect unresolved features in the model had on the solution. From these studies the mean rms errors in the reference level velocities and vertical mixing terms were estimated to be $\delta u_0 = \pm 0.6$ cm s^{-1}, $\delta v_0 = \pm 0.6$ cm s^{-1}, $\delta w_0 = \pm 2 \times 10^{-6}$ m s^{-1}, $\delta k_h = 1000$ m^2 s^{-1} in the upper 600 m, 2500 m^2 s^{-1} below 600 m, and $\delta k_z = 0$ to 6 cm^2 s^{-1} increasing with depth.

The vertical mixing coefficients determined by the model increased with depth from 0 cm^2 s^{-1} at 150 m

to 14 $cm^2 s^{-1}$ at 1500 m. The structure of the vertical diffusivity was consistent, with the vertical diffusivity being inversely related to the bouyancy frequency as suggested by Gargett (1984). The horizontal diffusivity had two distinct features, a decrease in diffusivity with depth in the upper 600 m and an increase in diffusivity from 700 m to 1000 m. The vertical velocity field determined from the model was a weak function of depth, implying that the horizontal velocities were nearly nondivergent.

The steady-state geostrophic flow field determined using the inverse solution revealed the presence of mesoscale eddies in the flow. However, the pattern of the flow thus determined was still generally smooth with well-defined flow features. At the surface, the inversion results produced the major features of the horizontal flow field evident in the raw drifter data but possessed much less eddy energy than the drifter data. In the halocline (100–200 m), the flow field from the model showed the existence of the oceanic front that was clearly present in the temperature and salinity fields (Matear et al. 1992). For depths greater than 1000 m, the horizontal flow field obtained from the inverse model gave a better defined flow pattern than assuming a depth of no motion. The flow in the OSE area did not exhibit a depth of no motion.

Current meter observations from the center of the grid contained small-scale eddy features that were not evident in the CTD data. This makes it difficult to use the current meter observations to determine the geostrophic reference velocity. From the current meter observations, the eddy energy appeared to be concentrated in the upper 200 m of the ocean. An increase in eddy energy at 1000 m was consistent with the calculated horizontal diffusivities.

Acknowledgments. I would like to thank Dr. S. Tabata for providing the CTD data, Dr. M. Levine and Dr. C. Paulson for granting the use of the current meter observations, and Dr. W. Large for allowing use of the mixed-layer drifter data. This work was supported by the Canadian Natural Sciences and Engineering Research Council and the Department of Fisheries and Oceans through grants to W. Hsieh and G. A. McBean.

REFERENCES

D'Asaro, E., P. Niiler, C. Erikson, and R. Davis, 1993: Low and inertial frequency currents in the mixed layer during October 1987 at Ocean Storms. *J. Phys. Oceanogr.*, **23**, in press.

Fleagle, R. G., M. Miyake, J. F. Garrett, and G. A. McBean, 1982: Storm transfer and response experiment. *Bull. Amer. Meteor. Soc.*, **63**, 6–14.

Fofonoff, N. P., and S. Tabata, 1966: Variability of oceanographic conditions between Ocean Station P and Swiftsure Bank off the Pacific coast of Canada. *J. Fish. Res. Board Can.*, **23**, 825–868.

——, and R. Millard, Jr., 1983: Algorithms for computation of fundamental properties of seawater. UNESCO Tech. Paper Marine Science, No. 44, 55 pp.

Gargett, A., 1984: Vertical eddy diffusivity in the ocean interior. *J. Mar. Res.*, **42**, 359–393.

Gregg, M., 1989: Scaling turbulent dissipation in the thermocline. *J. Geophys. Res.*, **94**, 9686–9698.

Lawson, C. L., and R. J. Hanson, 1974: *Solving Least Squares Problem.* Prentice-Hall, 340 pp.

Matear, R., 1989: Circulation of the northeast Pacific Ocean inferred from temperature and salinity data, M.Sc. thesis, Department of Geophysics, University of British Columbia, 121 pp.

——, G. A. McBean, and W. W. Hsieh, 1992: Hydrography and heat and salt budgets of the Ocean Storms area in autumn, 1987. *Atmos. Ocean,* submitted.

Menke, W., 1984: *Geophysical Data Analysis, Discrete Inverse Theory.* Academic Press, 260 pp.

Montgomery, R., 1938: Circulation in the upper layers of southern North Atlantic deduced with entropic analysis. Papers on Physical Oceanography and Meteorology, Massachusetts Institute of Technology and Woods Hole Oceanography Institution, 6(2).

Olbers, D. J., M. Wenzel, and J. Willebrand, 1985: The inference of North Atlantic circulation patterns form climatological hydrographic data. *Rev. Geophys.*, **23**, 313–356.

Tabata, S., 1961: Temporal changes of salinity, temperature, and dissolved oxygen content of the water at Station P in the northeast Pacific, and some of their determining Factors. *J. Fish. Res. Board Can.*, **18**, 1073–1124.

——, 1965: Variability of oceanographic conditions at Ocean Station P in the northeast Pacific Ocean. *Trans. R. Soc. Can.*, **III**, Series IV, (4), 367–418.

——, 1976: The general circulation of the Pacific Ocean and a brief account of the oceanographic structure of the North Pacific Ocean. Part II: Thermal regime and influence on the climate. *Atmosphere,* **14**, 1–27.

——, L. A. F. Spearing, R. H. Bigham, B. G. Minkley, J. Love, D. Yelland, J. Linguanti, and P. M. Kimber, 1988: STP/Hydrographic Observations along line P, Station P, line R and associated lines in the "Ocean Storms" Area: Cruise I: 22 Sept.–16 Oct. 1987, Cruise III: 24 Nov.–9 Dec. 1987., Canadian Data Report of Hydrography and Ocean Science, 70 pp.

Tziperman, E., and A. Hecht, 1988: Circulation in the eastern Levantine Basin determined by inverse methods. *J. Phys. Oceanogr.*, **18**, 506–518.

Wiggins, R. A., 1972: The general linear problem: Implication of surface waves and free oscillations for earth structure. *Rev. Geophys. Space Phys.*, **10**, 251–285.

Wunsch, C., 1978: The general circulation of the North Atlantic west 50°W determined from inverse methods. *Rev. Geophys.*, **16**, 583–620.

——, 1985: Can a tracer field be inverted for velocity? *J. Phys. Oceanogr.*, **15**, 1521–1531.

——, and J. Minister, 1982: Methods for box models and ocean circulation tracers: Mathematical programming and nonlinear inverse theory. *J. Geophys. Res.*, **87**, 5647–5662.